Ceramics International 43 (2017) 7065–7072

Contents lists available at ScienceDirect

Ceramics International

journal homepage: www.elsevier.com/locate/ceramint

Phase structural transition and microwave dielectric properties in isovalently substituted $La_{1-x}Ln_xTiNbO_6$ (Ln=Ce, Sm) ceramics

Jian Zhang, Ruzhong Zuo*

Institute of Electro Ceramics & Devices, School of Materials Science and Engineering, Hefei University of Technology, Hefei 230009, PR China

ARTICLE INFO

Keywords:
A. Sintering
B. X-ray methods
C. Dielectric properties

ABSTRACT

Aeschynite-type $La_{1-x}Ln_xTiNbO_6$ (Ln=Ce, Sm, x=0–1) ceramics were prepared via a conventional solid state method. Analysis of X-ray diffraction, Raman, infrared reflectivity spectra and the microstructures revealed a series of composition-induced phase evolution in sequence: monoclinic→coexistence of monoclinic and orthorhombic→orthorhombic structure, *i.e.* M→M+O→O. The critical compositions of distinguishing the dominant M or O phase were x=0.15 in $La_{1-x}Ce_xTiNbO_6$ and x=0.10 in $La_{1-x}Sm_xTiNbO_6$ ceramics, exactly corresponding to the average ionic radius of rare earth ions (IR) ~1.027 Å. The crystal structure and microwave dielectric properties of $RETiNbO_6$ (RE=rare earth) ceramics strongly depended on IR. Near-zero τ_f was achieved in the Ce-sample with x=0.153 (ε_r=28.9, Q×f=17,275 GHz@6.54 GHz) as well as in the Sm-sample with x=0.098 (ε_r=28.2, Q×f=19,186 GHz@6.78 GHz). Eventually, $RETiNbO_6$ would form O euxenite ($-\tau_f$), O aeschynite ($+\tau_f$), and M aeschynite ($-\tau_f$), as IR < 0.945 Å, 0.945 Å < IR < 1.027 Å, and 1.027 Å < IR < 1.032 Å, respectively. The infrared reflectivity study also confirmed that the structural phonon oscillations in the infrared region dominated the dielectric performance in the microwave region for this system.

1. Introduction

A growing requirement for dielectric resonator materials has been stimulated by the rapid development of wireless communication systems and microwave integrated circuit technology [1–3]. A series of microwave dielectric ceramics $RETiNbO_6$ (RE=rare earth) were firstly reported by Sebastian et al. [4] Interestingly, compounds with atomic numbers of RE ions in the range 58–63 have an orthorhombic (O) aeschynite structure with a *Pnma* space group (Z=4). However, compounds with atomic numbers of RE ions in the range of 64–71, have an O euxenite structure with a *Pbcn* space group (Z=4). The essential difference between the above two structures is that RE ions lie in the closely-connected chains for aeschynites but on the closely-packed parallel planes for euxenites. Ceramics with an aeschynite structure were reported to possess a positive temperature coefficient of resonant frequency τ_f and a high permittivity ε_r while ones with a euxenite structure have a negative τ_f and a relatively low ε_r. $RETiNbO_6$ ceramic materials with near-zero τ_f values were investigated systematically by Surendran et al. via preparing solid solutions between aeschynite and euxenite [5].

Among these $RETiNbO_6$ compounds, $LaTiNbO_6$ belongs to a special one, and generally exhibits a monoclinic (M) aeschynite structure with a *C*2/*c* space group [6]. However, it has received little attention perhaps due to its moderate microwave dielectric properties of ε_r=22.3, Q×f=49,867 GHz, τ_f=−55 ppm/°C [6]. In our previous work [7], an M-O phase transition was induced in $LaTiNbO_6$ by an annealing process, accompanying adjustable microwave dielectric properties. Big differences in microwave dielectric properties between M and O aeschynite ceramics, especially their opposite τ_f values, stimulated us to explore whether isovalent substitution at La-sites of $LaTiNbO_6$ could induce a similar phase transition or not, and how it would affect the final microwave dielectric properties. In this work, Ce^{3+} and Sm^{3+} were chosen as the substitution ions because $SmTiNbO_6$ and $CeTiNbO_6$ were two typical O aeschynite compounds in $RETiNbO_6$ family.

The sintering behavior, phase composition, microstructure and microwave dielectric properties of $La_{1-x}Ln_xTiNbO_6$ (Ln=Ce, Sm, 0≤x≤1) ceramics were studied systematically by means of X-ray diffraction (XRD), scanning electron microscopy (SEM), Raman, infrared reflectivity spectra and so on.

2. Experimental procedure

$La_{1-x}Ln_xTiNbO_6$ (Ln=Ce, Sm, x=0–1) ceramics were prepared by a routine solid-state reaction process. High-purity (> 99%) La_2O_3, CeO_2, Sm_2O_3, Nb_2O_5 and TiO_2 powders were used as the starting materials. The La_2O_3, CeO_2 and Sm_2O_3 powders were pretreated at 800 °C in air

* Corresponding author.
E-mail address: rzzuo@hotmail.com (R. Zuo).

http://dx.doi.org/10.1016/j.ceramint.2017.02.136
Received 10 February 2017; Received in revised form 24 February 2017; Accepted 25 February 2017
Available online 27 February 2017

for 2 h to remove any hydroxides before weighing. The raw powders of stoichiometric proportion were weighed and then ball milled using zirconia balls in ethanol medium for 4 h. The resultant slurry was then dried and calcined at 1250 °C for 4 h, followed by a second grinding process for 6 h. The reground powders were mixed with 5 wt% PVA binders, and then pressed into cylinders with 10 mm in diameter and 5–6 mm in height under a uniaxial pressure of 200 MPa. The specimens were first heated at 550 °C for 4 h at 3 °C/min to burn out the organic binder, and then sintered in the temperature range of 1300–1450 °C for 4 h at 5 °C/min in ambient atmosphere.

The crystalline structures of the sintered samples were determined by an X-ray diffractometer (D/Max2500V, Rigaku, Tokyo, Japan) using Cu Kα radiation. Prior to the examination, the sintered pellets were crushed into powders with a mortar. The diffraction patterns were obtained over a 2θ range of 10–90° with a step of 0.02°. The data were performed by the Rietveld refinement method, using GSAS suite equipped with EXPGUI software [8,9]. The bulk densities of the sintered ceramics were measured using the Archimedes method. The microstructure observation of the post-sintered pellets and the quantitative analysis of elements in different grains were performed using SEM (JEOL JSM-6490LV, Tokyo, Japan) equipped with an energy dispersive spectrometer (EDS). Raman spectra were collected at room temperature using a Raman spectrometer (532 nm, LabRAM HR800, HJY, Longjumeau Cedex, France). Room-temperature infrared reflectivity spectra were measured by using a Bruker IFS 66v FTIR spectrometer (IFS 66v/S Vacuum; Bruker Optik GmbH, German) on Infrared beamline station (U4) at the National Synchrotron Radiation Laboratory (NSRL), Hefei, China. A network analyzer (Agilent, N5230C, Palo Alto, CA) and a temperature chamber (GDW-100, Saiweisi, Changzhou, China) were used to measure the dielectric properties of the well-polished ceramic samples by means of a Hakki-Coleman post resonator method [10,11]. The τ_f values of the samples were measured in the temperature range from 20 °C to 80 °C. It can be calculated as follows: $\tau_f=(f_2-f_1)/f_1(T_2-T_1)$, where f_1 and f_2 represent the resonant frequencies at T_1 and T_2, respectively.

3. Results and discussion

$LnTiNbO_6$ (Ln=Ce, Sm) ceramics have an O aeschynite structure with a *Pbnm* space group [4]. They could be well sintered at high temperatures above 1300 °C. However, $LaTiNbO_6$ is generally in the form of M phase with a *C2/c* space group because there is an O-M phase transition at 1230 °C [12]. Fig. 1 shows normalized XRD patterns of $La_{1-x}Ln_xTiNbO_6$ (Ln=Ce, Sm) ceramics. It could be seen that all peaks of $ReTiNbO_6$ (Re=La, Ce, and Sm) could be well indexed to the patterns of JCPDS files #15-0872, 15-0864, and 20-1470, respectively. An obvious structure transformation from M to O could be observed in Ce- or Sm-substituted $LaTiNbO_6$ ceramics. It occurred when x > 0.05, and finished at x=0.3 and x=0.2 in $La_{1-x}Ce_xTiNbO_6$ and $La_{1-x}Sm_xTiNbO_6$ ceramics, respectively. M-phase and O-phase zones were respectively highlighted by magenta and yellow. The cyan region corresponded to the coexistence zone of M and O phases, in which the relative content of O phase increased with increasing x.

To further study the phase composition and crystal structure, refinements were carried out using GSAS software. $LaTiNbO_6$ (ICSD #413439) [13] and $CeTiNbO_6$ (ICSD #20600) [14] were adopted as the initial models for M and O phase, respectively. The ion occupancy in the two models was revised according to the nominal composition before the refinement. Detailed structural parameters, reliability factors and goodness-of-fit indicator of $La_{1-x}Ln_xTiNbO_6$ ceramics are listed in Table 1. The refinement plots of $La_{0.85}Ce_{0.15}TiNbO_6$ and $La_{0.9}Sm_{0.1}TiNbO_6$ ceramics are also representatively given in Fig. 2. It could be noted that the observed and calculated diffraction profiles kept a good consistency, as confirmed by the relatively low amplitudes of the difference lines (blue lines in Fig. 2). The refinement reliable factors of R_{wp}, R_p, and χ^2 were found to be in the range of 9–11%, 7–9%, and 1.4–1.7, respectively, indicating that the structural model was valid and the refinement result was reliable. As can be seen from Table 1, the relative content of M phase decreased and O phase increased with increasing x until the matrix was completely full of O phase as x≥0.3 in $La_{1-x}Ce_xTiNbO_6$ and x≥0.2 in $La_{1-x}Sm_xTiNbO_6$ ceramics. In addition, the lattice parameters and cell volumes in M (or O phase) slightly decreased with increasing the Ce or Sm content, which could be ascribed to the smaller ionic radius of Ce^{3+} (1.01 Å) or Sm^{3+} (0.958 Å) than that of La^{3+} (1.032 Å) at a coordination number of 6 [15]. Although the starting powder CeO_2 was used, yet Ce^{3+} should exist in $La_{1-x}Ce_xTiNbO_6$ ceramics according to the literature work [16], in which only completely reduced Ce^{3+} cations in $CeTiNbO_6$ and $CeTiTaO_6$ ceramics after a conventional air sintering was identified by an X-ray photoelectron spectroscope.

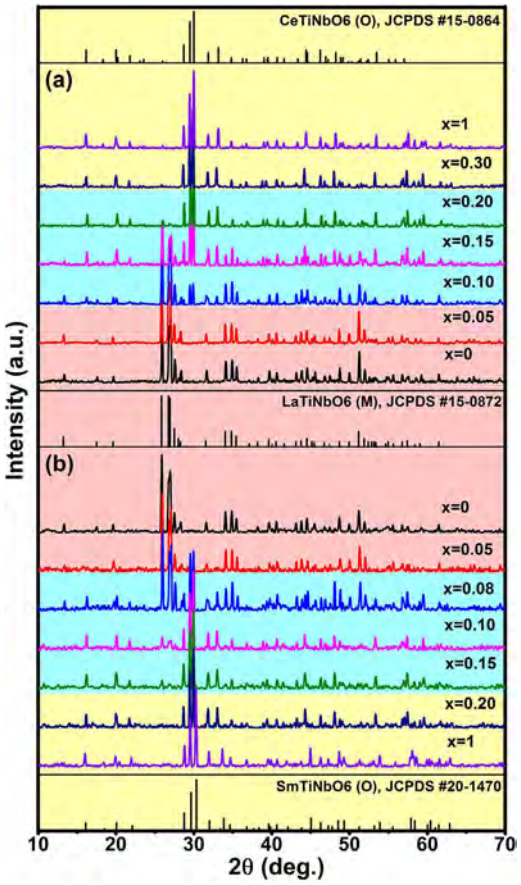

Fig. 1. XRD patterns of (a) $La_{1-x}Ce_xTiNbO_6$ and (b) $La_{1-x}Sm_xTiNbO_6$ ceramics sintered at optimal temperatures.

Raman spectroscopy is a powerful tool to provide the information that correlates vibrational characteristics to microwave dielectric properties [17]. It is easy to find in Fig. 3(a) that the Raman spectra of two end compositions $LaTiNbO_6$ and $CeTiNbO_6$ in $La_{1-x}Ce_xTiNbO_6$ ceramics were completely different, which confirmed their different crystal structures. In fact, $LaTiNbO_6$ and $CeTiNbO_6$ crystals consisted of identical structural unit $(Ti, Nb)_2O_{10}$ by different ways of connection. According to previous literatures on similar structure [18–20], it was possible to separate the spectra of our materials in some regions with specific modes. The bands with wavenumbers larger than 450 cm^{-1} can be associated with several modes involving the stretching of the (Nb,Ti)–O bonds, and the bands with wavenumbers between 200 and 450 cm^{-1} are due principally to the bending of O–(Nb,Ti)–O bonds and the stretching RE-O vibrations. The origin of the bands with wavenumbers below 200 cm^{-1} should be lattice vibrations caused by RE ions. Raman shifts of the x=0.05 sample were similar to those of pure $LaTiNbO_6$ ceramic, suggesting that a single M-phase solid

Table 1
Refined lattice parameters of $La_{1-x}Ln_xTiNbO_6$ ceramics.

$La_{1-x}Ce_xTiNbO_6$								$La_{1-x}Sm_xTiNbO_6$					
x	0	0.05	0.10	0.15	0.20	0.30	1	0.05	0.08	0.10	0.15	0.20	1
M (wt%)	100	100	82.0(1)	41.0(5)	5.3(5)	0	0	100	62.6(4)	22.4(8)	8.8 (2)	0	0
O (wt%)	0	0	18.0(4)	59.0(3)	94.7(4)	100	100	0	37.4(5)	77.6(2)	91.2(1)	100	100
M phase													
a (Å)	11.195(2)	11.1819(5)	11.1761(6)	11.170(1)	11.16(1)	–	–	11.170(4)	11.165(5)	11.161(2)	11.17(1)	–	–
b (Å)	8.842(2)	8.8344(4)	8.8346(5)	8.8347(9)	8.839(9)	–	–	8.834(4)	8.835(4)	8.831(2)	8.81(1)	–	–
c (Å)	5.268(1)	5.2655(2)	5.2647(3)	5.2649(5)	5.267(6)	–	–	5.265(2)	5.264(3)	5.264(1)	5.258(7)	–	–
α=β (°)	90	90	90	90	90	–	–	90	90	90	90	–	–
γ (°)	115.333(2)	115.335(2)	115.341(3)	115.346(6)	115.45(6)	–	–	115.351(5)	115.356(5)	115.38(1)	115.33(8)	–	–
V ($Å^3$)	471.4(3)	470.13(4)	469.80(5)	469.58(6)	469.4(5)	–	–	469.6(5)	469.3(6)	468.8(1)	468.4(7)	–	–
O Phase													
a (Å)	–	–	5.4386(5)	5.4372(3)	5.4355(2)	5.4343(7)	5.3955(2)	–	5.435(2)	5.4298(3)	5.4222(4)	5.4141(4)	5.297(2)
b (Å)	–	–	10.9340(9)	10.9349(6)	10.9356(4)	10.935(1)	10.9418(5)	–	10.946(4)	10.9391(5)	10.9344(8)	10.9316(9)	10.968(3)
c (Å)	–	–	7.5716(6)	7.5707(3)	7.5689(3)	7.568(1)	7.5320(3)	–	7.574(2)	7.5662(3)	7.5575(5)	7.5501(6)	7.456(2)
α=β=γ (°)	–	–	90	90	90	90	90	–	90	90	90	90	90
V ($Å^3$)	–	–	450.26(6)	450.12(5)	449.90(4)	449.8(2)	444.67(4)	–	450.6(4)	449.42(5)	448.08(7)	446.85(9)	433.2(4)
R_{wp} (%)	9.71	9.24	9.23	9.9	10.28	10.01	11.64	10.11	11.78	11.86	9.94	10.48	10.9
R_p (%)	7.64	7.24	7.22	7.84	8.15	7.88	9.27	8.02	9.23	9.33	7.82	8.24	8.68
χ^2 (%)	1.498	1.524	1.563	1.617	1.717	1.64	1.506	1.458	1.551	1.589	1.437	1.484	1.318

V: unit cell volume.

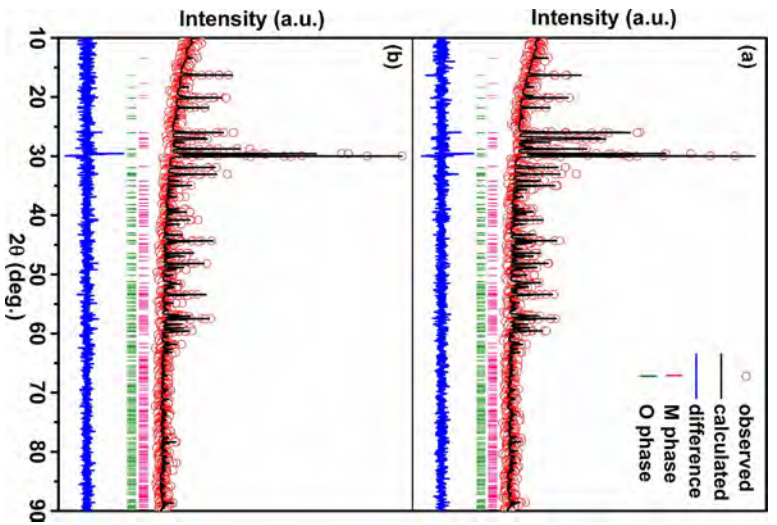

Fig. 2. Rietveld refinement plots of (a) $La_{0.85}Ce_{0.15}TiNbO_6$ and (b) $La_{0.9}Sm_{0.1}TiNbO_6$ ceramics. (For interpretation of the references to color in this figure, the reader is referred to the web version of this article.)

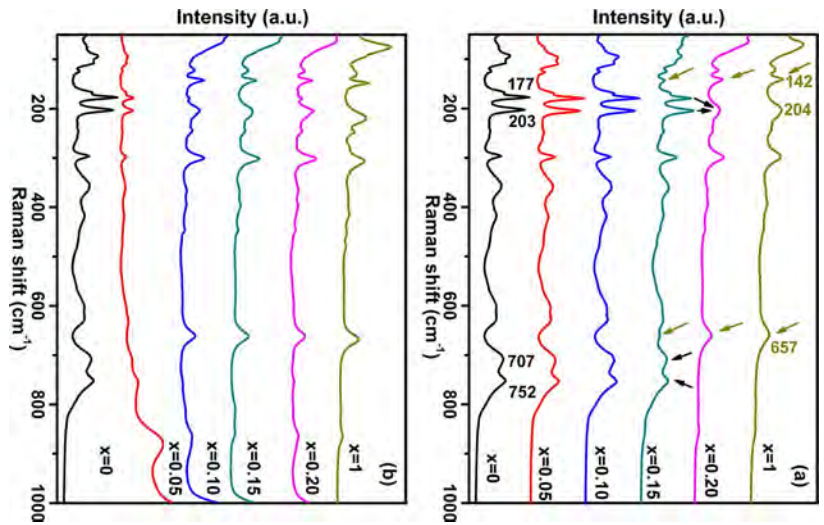

Fig. 3. Raman spectra of (a) $La_{1-x}Ce_xTiNbO_6$ and (b) $La_{1-x}Sm_xTiNbO_6$ ceramics sintered at optimal temperatures.

solution was formed. When x increased up to 0.10, an obvious broadening was observed nearly for all Raman peaks. These might be closely related to the decay of microwave propagation and the large structural distortion caused by the substitution of ions with different radii [21–23]. Besides, new Raman peaks at 142 and 657 cm^{-1} appeared in x=0.15 sample, as marked by arrows. Their intensity increased gradually with increasing the Ce content. The mode of 657 cm^{-1} was originated from the stretching of oxygen-bridged bonds or (Nb,Ti)-O-(Nb,Ti), O-(Nb,Ti)-O chains, which was the feature of O structure [19,20]. These apparently indicated the coexistence of M and O phases in the ceramics. With further increasing x to 0.20, Raman modes of 177 and 203 cm^{-1} merged into a single one at 204 cm^{-1} together with the disappearance of modes at 707 and 752 cm^{-1}. These variations in low wavenumber were primarily attributed to the lattice vibrations caused by the substitution of Ce^{3+} for La^{3+}. Although there was still 5% residual M phase (as shown in Table 1), the x=0.2 ceramic showed similar Raman shifts to the pure $CeTiNbO_6$ ceramic, indicating the formation of O-phase solid solution. By comparison, the variation of the Raman shifts in $La_{1-x}Sm_xTiNbO_6$ ceramics, is more drastically than that in $La_{1-x}Ce_xTiNbO_6$ ceramics, as shown in Fig. 3(b). The reason might be that a larger lattice distortion could accelerate the phase transition of the matrix composition as a result of larger ion radius difference between Sm^{3+} and La^{3+}. Nevertheless, Raman results kept good consistency with the XRD data, both of which confirmed the as-mentioned composition induced M-O phase transition process.

The typical SEM images of $La_{1-x}Ln_xTiNbO_6$ (Ln=Ce, Sm, x=0–1) ceramics sintered at optimal temperatures are shown in Fig. 4. As can be seen from Fig. 4(a)–(c), polygonal grains in size of ~10×10 μm^2, short rod-like grains in size of ~5×2 μm^2, and slightly cubic-like grains in size of ~2×2 μm^2 could be seen in un-doped $LaTiNbO_6$, $CeTiNbO_6$, and $SmTiNbO_6$ ceramics, respectively. Although the polygonal grain morphology of $La_{1-x}Ce_xTiNbO_6$ was maintained till x=0.15, the grain size abruptly increased to ~120×120 μm^2 at x=0.05 and almost unchanged up to x=0.15, as can be seen from Fig. 4(d)–(f). In this composition range, all specimens exhibited a dense microstructure without obvious pores. In addition to the x=0.05 composition, a few tiny particles were observed to appear at the grain boundary and they became more and more with increasing x from 0.10 to 0.15. As $x \geq 0.3$, the ceramics kept a short rod-like morphology of undoped $CeTiNbO_6$, which conformed to the fact that these compositions belong to single O-phase solid solutions (as discussed in Fig. 1). The grain size slightly increased with increasing the Ce content. As $0.15 < x < 0.3$, the $La_{1-x}Ce_xTiNbO_6$ sample exhibited extremely non-uniform microstructure. A small amount of abnormally large grains appeared in the fine matrix grains. This kind of bimodal grain morphology might be due to the M-O phase coexistence in the range of $0.1 \leq x < 0.3$. By contrast, the effect of Sm substitution for La on the microstructure of $LaTiNbO_6$ ceramics was more obvious, as observed from Fig. 4(i–l). After 10% La was replaced by Sm, extremely large grains started to be observed in the fine cubic-like matrix grains. This kind of bimodal grain distribution can be observed till the Sm content is 0.15. As $x \geq 0.2$, the $La_{1-x}Sm_xTiNbO_6$ ceramics exhibited single cubic-like grains similar to those of undoped $SmTiNbO_6$, probably because all of them belonged to a single O-phase structure. For both cases of Sm- or Ce-substituted $LaTiNbO_6$ ceramics, the formation of this special two-phase grain morphology can be considered as a result of the abnormal growth of large La-rich M-phase polygonal grains in fine O-phase Ce-rich short rod-like grains or Sm-rich cubic-like grains, which conformed to the Ostwald ripening mechanism. It is a pity that EDS can not be used to distinguish the above two phases because of almost identical compositions in these samples, similar to the case of previously reported $Bi_{1-x}Ce_xVO_4$ solid solution ceramics [24].

Microwave dielectric properties and density of $La_{1-x}Ce_xTiNbO_6$ (x=0–1) ceramics as a function of x are shown in Fig. 5(a). There were three stages of change in ε_r and τ_f when x increased, exactly corresponding to the above-mentioned three phase zones. First, single-M zone ($0 \leq x \leq 0.05$). ε_r decreased from 22.5 to 15.9 but τ_f remained a constant (~−54 ppm/°C) with 5% Ce substitution. As is well known, τ_f mainly depends on intrinsic structure but ε_r is closely related to the densification, ionic polarizability, porosity, secondary phase and structural characteristics such as the distortion, tilting, and/or rattling spaces of oxygen octahedron in the unit cell. The variation of ε_r with increasing x was consistent with that of density in current work. It is worth noting that the samples are difficult to sinter near the starting composition of the phase transition (x=0.05) with unknown reasons, similar to the sharp change near the transition point in $RE_{1-x}RE'_xTiNbO_6$ ceramics [5]. Hence, the poor densification might be responsible for the decreased ε_r values, and the identical structure contributed to the unchanged τ_f values in this stage. Secondly, M-O coexistence zone ($0.05 < x < 0.30$). As x increased, ε_r and τ_f respectively increased to 63.4 and 111.2 ppm/°C in the same pace, which conformed to the two-phase mixing rule. This synchronous change in ε_r and τ_f was closely related to their correlated dielectric response mechanism in the material, similar to the variation reported in previous work [25,26]. Thirdly, single-O zone ($0.30 \leq x \leq 1$). ε_r and τ_f monotonically decreased to 60 and 83 ppm/°C gently with the increment of Ce content, respectively. In addition, it can be found from the inset of Fig. 5(a), the Q×f values of the whole composition abruptly decreased from 68,000 to 13,000 GHz when x increased to 0.3, then remained stable, which mainly caused by the formation of high-loss O phase. Similar variation of microwave properties in $La_{1-x}Sm_xTiNbO_6$ (x=0–1) is also illustrated in Fig. 5(b). It is noteworthy that the abrupt changes of microwave dielectric properties were located in 15% Ce-substituted and 10% Sm-substituted $LaTiNbO_6$ ceramics, which simultaneously corresponded to the approximate phase transition point as discussed in the section of XRD and Raman. It also implied that the substitution of Sm^{3+} was easier to induce the phase transition in $LaTiNbO_6$ than that of Ce^{3+}. Meanwhile, excellent microwave dielectric properties of ε_r=28.9, Q×f=17,275 GHz@6.54 GHz and τ_f=−2 ppm/°C were achieved in the Ce-sample with x=0.153, and ε_r=28.2, Q×f=19,186 GHz@6.78 GHz and τ_f=−8 ppm/°C in the Sm-sample with x=0.098.

It is well known that the average ionic radius of RE ions (IR) plays an important role in the determination of structure and properties for RE compounds. To explore whether there is a critical radius to identify the dominant M or O phase, variations of ε_r and τ_f in $La_{1-x}Ln_xTiNbO_6$ ceramics as a function of IR were carefully plotted in Fig. 6. IR in current work was calculated using the data reported by Shannon et al. as the coordination number was six [15]. The ε_r and τ_f values showed a sharp and abrupt change when IR was ~1.027 Å, indicating the critical IR between M and O phase. The results clearly demonstrated that $La_{1-x}Ln_xTiNbO_6$ compounds were prior to crystallize in O phase for IR < 1.027 Å and in M phase for 1.027 Å < IR < 1.032 Å (the ionic radius of La^{3+} is 1.032 Å). Moreover, it can also be found from Fig. 6(b) that the sign of τ_f strongly depended on IR. For IR < 1.027 Å, the materials would have positive τ_f values and for 1.027 Å < IR < 1.032 Å the τ_f values would be negative. The results suggested that one could obtain a near-zero-τ_f material by adjusting IR to be ~1.027 Å in $RETiNbO_6$ compounds. However, it is regrettable that no cation has such a large ionic radius up to ~1.027 Å to give a direct proving. Surendran et al. [5] have also reported that a positive τ_f with O aeschynite-type $RETiNbO_6$ formed for IR > 0.945 Å and a negative τ_f with O euxenite-type $RETiNbO_6$ formed for IR < 0.945 Å. Therefore, it could be summarized that $RETiNbO_6$ would be in the form of O euxenite ($-\tau_f$), O aeschynite ($+\tau_f$), and M aeschynite ($-\tau_f$) as IR < 0.945 Å, 1.027 Å < IR < 1.032 Å, and 0.945 Å < IR < 1.027 Å, respectively. The current work further enriched and perfected the relationship between phase structure and IR in $RETiNbO_6$ system.

To better understand the microwave dielectric behavior of $La_{1-x}Ln_xTiNbO_6$ ceramics, the infrared reflectivity spectra are demonstrated in Fig. 7. Obviously, the end compositions x=0 ($LaTiNbO_6$) and x=1 ($CeTiNbO_6$ or $SmTiNbO_6$) presented completely different spectra

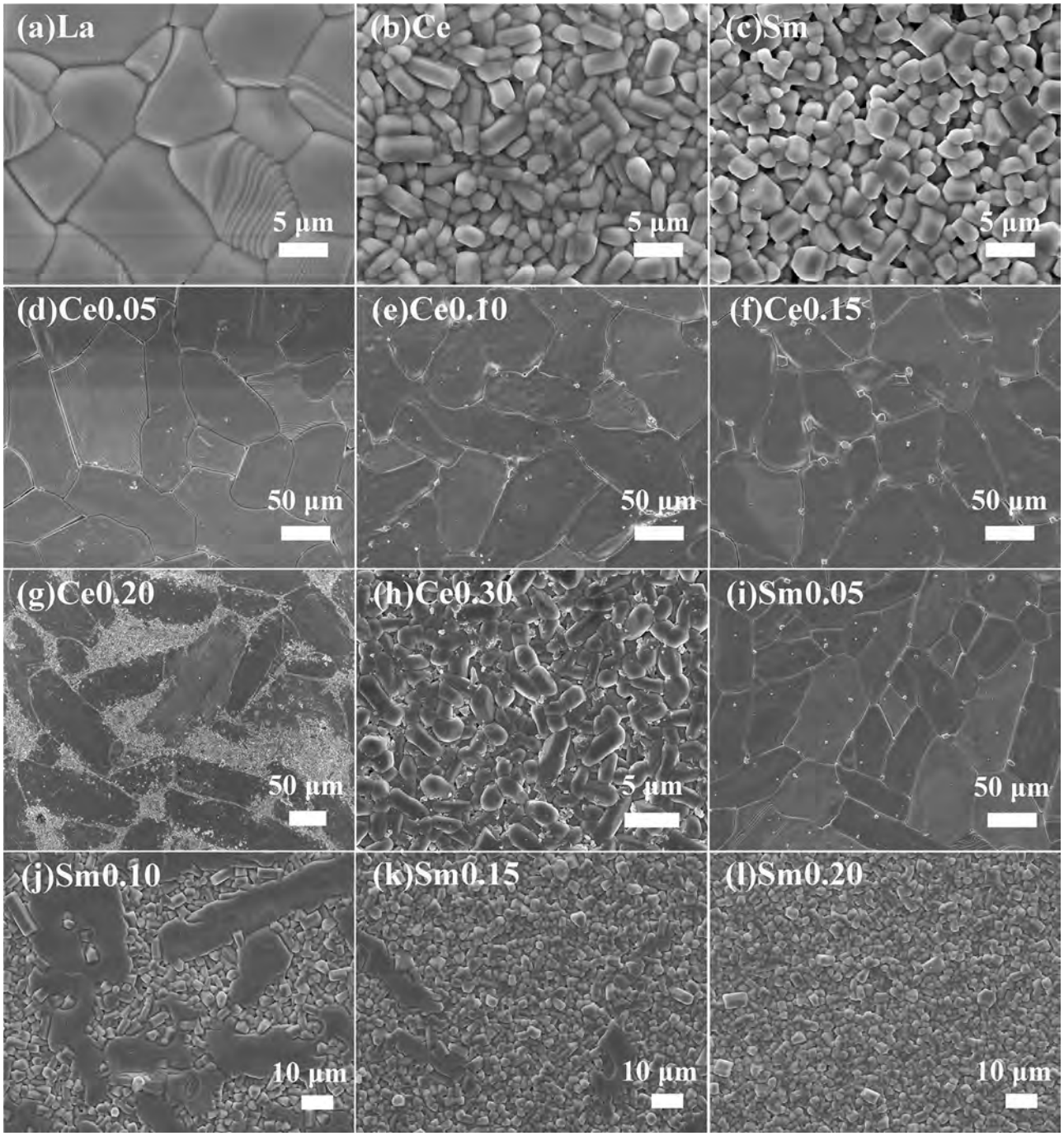

Fig. 4. SEM images of the $La_{1-x}Ln_xTiNbO_6$ ceramics sintered at 1375 °C for 4 h: (a) $LaTiNbO_6$; (b) $CeTiNbO_6$; (c) $SmTiNbO_6$; (d) Ce-0.05; (e) Ce-0.10; (f) Ce-0.15; (g) Ce-0.20; (h) Sm-0.05; (i) Sm-0.10; (j) Sm-0.15; (k) Sm-0.20.

due to their different phase structures, especially as the wavenumber < 500 cm^{-1}. To put it simple, modes 1 and 3 (as marked in Fig. 7) could be regarded as the typical modes in O phase, and mode 2 could stand for M phase. It can be observed in Fig. 7(a) that mode 2 in the x=0.05 sample was almost the same with that of x=0, then became broaden as x increased to 0.15, and then disappeared while the new modes 1 and 3 appeared when x≥0.20, corresponding to the phase evolution of M→M +O→O. By contrast, as seen in Fig. 7(b), mode 2 has been broadened at x=0.05 in $La_{1-x}Sm_xTiNbO_6$, and disappeared when x=0.10, then modes 1 and 3 increased as x further increased. In addition, modes 4 and 5 also slightly shifted to high wavenumbers with increasing x in both $La_{1-x}Ce_xTiNbO_6$ and $La_{1-x}Sm_xTiNbO_6$ ceramics, which might be attributed to the lattice distortion from ion substitution [27]. The evolution of infrared reflectivity spectra with increasing x was exactly the same as that of Raman spectra and in accordance with the structural changes discussed in the previous sections. It was confirmed again that Sm^{3+} substitution was easier to induce the phase transition in $LaTiNbO_6$ ceramics than Ce^{3+}.

These spectra have been further analyzed by using the four-parameter semiquantum model [28–31], and a nonlinear least-squares program [32]. According to this model, the infrared phonon contribution to the complex dielectric function ε(ω) is given by:

$$\varepsilon(\omega) = \varepsilon_\infty \prod_{j=1}^{N} \frac{\Omega_{j,LO}^2 - \omega^2 + i\omega\gamma_{j,LO}}{\Omega_{j,TO}^2 - \omega^2 + i\omega\gamma_{j,TO}} \quad (1)$$

where ε_∞ is the dielectric constant due to the electronic polarization

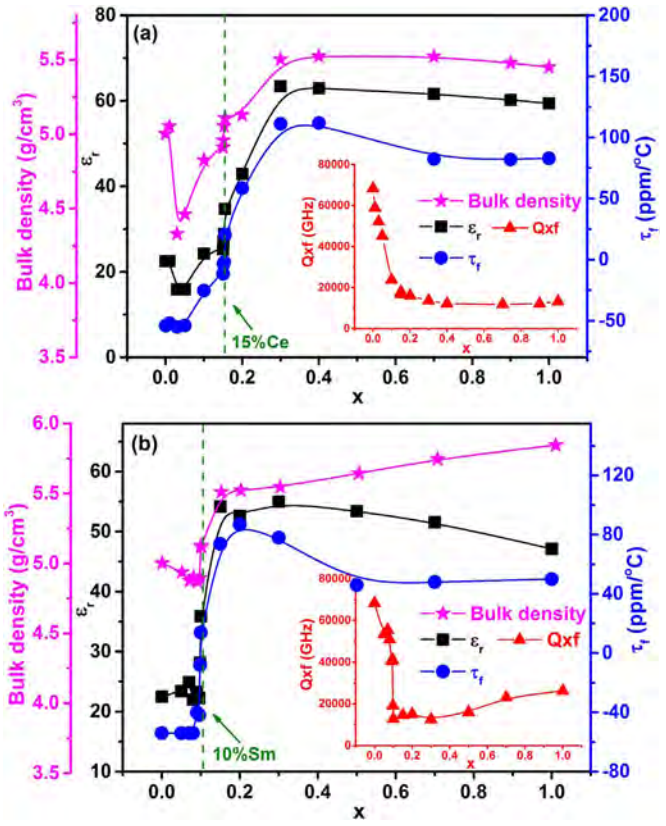

Fig. 5. The microwave dielectric properties and density of (a) $La_{1-x}Ce_xTiNbO_6$ and (b) $La_{1-x}Sm_xTiNbO_6$ ceramics sintered at optimal temperatures.

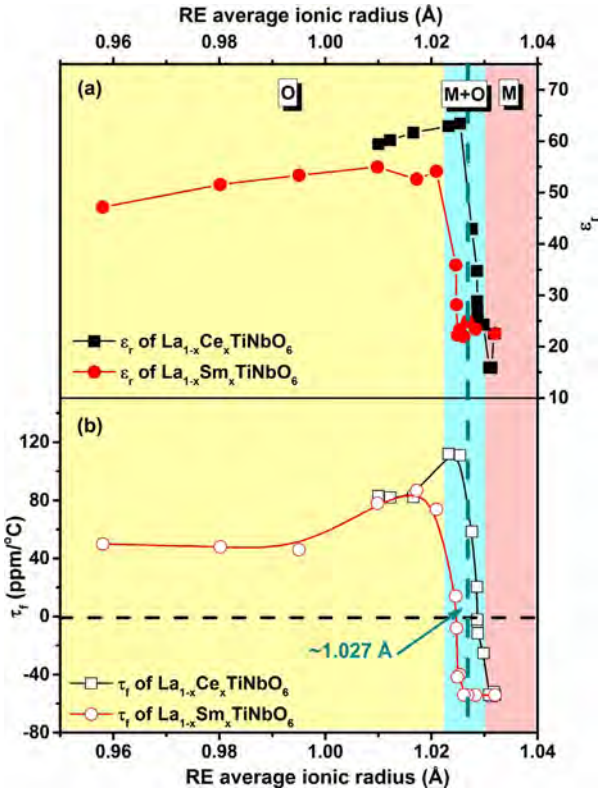

Fig. 6. Variation of (a) ε_r and (b) τ_f with average ionic radius of the rare earth in $La_{1-x}Ln_xTiNbO_6$ ceramics.

contribution, $\Omega_{j,\ LO}$ ($\Omega_{j,\ TO}$) and $\gamma_{j,\ LO}$ ($\gamma_{j,\ TO}$) are the frequency and damping of the jth longitudinal (transverse) optical modes, respectively, N is the number of polar phonons. At quasinormal incidence, the dielectric function is related to the optical reflectivity R by the Fresnel formula

$$R(\omega) = \left| \frac{1 - \sqrt{\varepsilon(\omega)}}{1 + \sqrt{\varepsilon(\omega)}} \right|^2 \tag{2}$$

Eqs. (1) and (2) are used to fit the experimental data and the results are also presented in Fig. 7. It can be clearly seen that the curves fitted the data of experiments very well, indicating that the model is valid.

Once the infrared modes are determined, the oscillator strengths of the individual *j*th TO modes can be obtained by [29–31]

$$\Delta\varepsilon_j = \frac{\varepsilon_\infty}{\Omega_{j,TO}^2} \times \frac{\prod_k (\Omega_{k,LO}^2 - \Omega_{j,TO}^2)}{\prod_{k\neq j} (\Omega_{k,TO}^2 - \Omega_{j,TO}^2)} \tag{3}$$

The static (infrared) dielectric constant ε_0, which corresponds to the intrinsic microwave dielectric constant, can be then obtained by adding the oscillator strengths over all modes [29–31], *i.e.*

$$\varepsilon_0 = \varepsilon_\infty + \sum_{j=1}^{N} \Delta\varepsilon_j \tag{4}$$

Besides, the dielectric loss tangent (tan δ) is given by adding the individual losses [31], that is,

$$\tan\delta = \sum_j \tan\delta_j = \sum_j \frac{\omega \triangle \varepsilon_j \gamma_{j,TO}}{\varepsilon_0 \Omega_{j,TO}^2} \tag{5}$$

The intrinsic (microwave-extrapolated) unloaded quality factor Q_u also can be estimated, which is the reciprocal of the dielectric loss tangent. As an example, the values of $\Delta\varepsilon_j$, ε_∞, ε_0, tan δ and $Q_u \times f$ (at 10 GHz) for $La_{0.85}Ce_{0.15}TiNbO_6$ together with the phonon mode parameters are listed in Table 2. Its dielectric permittivity at optical frequency was 2.88, and the extrapolated value in the microwave region was 26.37, which was in reasonable agreement with the measured value of 25.28. The dielectric polarization contribution from the first seven modes (120–268 cm^{-1}) was about 18.13, which was 69% of the total value. The accumulated tan δ value from the first seven modes was also 91% of the total value. Hence, it could be concluded that the polarization of current ceramics in the microwave region was due to the absorptions of phonon oscillations in the infrared region [33,34]. In addition, the microwave-extrapolated dielectric loss $Q_u \times f$ was 45,873 GHz, but the measured microwave dielectric loss Q×f of $La_{0.85}Ce_{0.15}TiNbO_6$ ceramic was 17,911 GHz ($Q_u \times f$ and Q×f are almost equivalent). The relative density of $La_{0.85}Ce_{0.15}TiNbO_6$ ceramic was about 90%. Thus, the difference between the estimated and measured dielectric loss might be mainly attributed to the extrinsic factor, such as density, pores, structural defects, *etc.* Efforts to analyse the vibrational and structural behaviors of these materials are in progress and it will be published elsewhere.

4. Conclusions

A series of $La_{1-x}Ln_xTiNbO_6$ (Ln=Ce, Sm, x=0–1) solid solutions were prepared via a conventional solid-state ceramic route. An M-O aeschynite transition occurred as $0.05 < x < 0.3$ in $La_{1-x}Ce_xTiNbO_6$ and $0.05 < x < 0.2$ in $La_{1-x}Sm_xTiNbO_6$ ceramics, while a single M or O phase region was formed at both ends, x=0 and x=1, respectively. M-phase ceramics generally had a low ε_r (~23), a negative τ_f (~−54 ppm/°C) and a large Q×f (~68,285 GHz), but O-phase ceramics owned a high ε_r (> 45), a positive τ_f (> 50 ppm/°C) and a low Q×f (< 30,000 GHz). An abrupt change of dielectric properties indicated that the boundary composition of the phase transition was at x=0.15 in $La_{1-x}Ce_xTiNbO_6$ and x=0.10 in $La_{1-x}Sm_xTiNbO_6$ ceramics at the

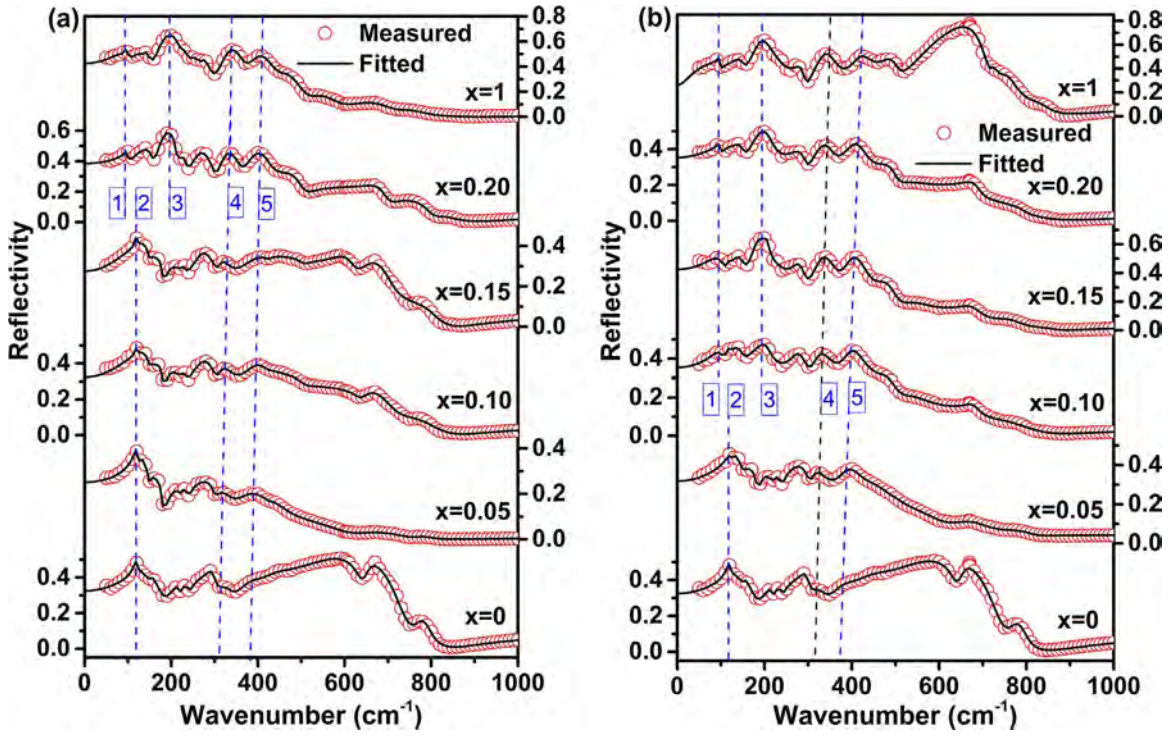

Fig. 7. Fitted and measured infrared reflectivity spectra of (a) $La_{1-x}Ce_xTiNbO_6$ and (b) $La_{1-x}Sm_xTiNbO_6$ ceramics at optimal temperatures.

Table 2
Infrared dispersion parameters, dielectric strengths and loss tangent obtained from the fitting of the infrared reflectivity spectrum of the $La_{0.85}Ce_{0.15}TiNbO_6$ ceramic[a].

Phonons	$\Omega_{j,\ TO}$ (cm^{-1})	$\gamma_{j,\ TO}$ (cm^{-1})	$\Omega_{j,\ LO}$ (cm^{-1})	$\gamma_{j,\ LO}$ (cm^{-1})	$\Delta\varepsilon_j$	10^6 tan δ_j/ω
1	120.25	13.51	123.32	12.77	3.43	121.53
2	134.22	20.50	143.91	23.05	5.52	238.20
3	154.50	25.58	160.58	24.80	2.11	85.75
4	167.66	20.55	178.01	29.79	1.52	42.14
5	206.18	24.09	213.09	26.52	1.46	31.38
6	229.14	24.67	236.11	31.23	1.09	19.42
7	268.15	38.28	296.23	75.78	3.00	60.57
8	322.37	48.13	333.65	88.41	0.61	10.71
9	395.66	53.33	416.80	84.73	1.43	18.47
10	447.77	48.72	462.05	76.60	0.59	5.44
11	490.99	40.23	496.61	49.57	0.23	1.46
12	539.26	66.12	555.53	72.25	0.81	6.98
13	584.66	65.75	613.92	79.07	0.77	5.62
14	657.88	84.17	711.41	88.00	0.71	5.24
15	776.67	86.72	800.10	58.87	0.20	1.09
ε_∞=2.88, ε_0=26.37, $Q_u \times f$= 45,873 GHz					Σtan δ_j/ω=654×10^{-6}	

[a] The phonon positions and damping constants are given in cm^{-1}.

optimal temperatures. The smaller Sm^{3+} substitution could induce the M-O phase transition in the $LaTiNbO_6$ more easily than Ce^{3+}. It was also found that the crystal structure and microwave dielectric properties of $RETiNbO_6$ ceramics strongly depended on IR. If 0.945 Å < IR < 1.027 Å, the system would crystallize in O aeschynite with a positive τ_f. If 1.027 Å < IR < 1.032 Å, the system would then crystallize in M aeschynite with a negative τ_f. This provides a method to design the materials with required performance by adjusting IR.

Acknowledgements

This work was financially supported by the National Natural Science Foundation of China (Grant No. 51272060).

References

[1] M. Makimoto, S. Yamashita, Microwave Resonators and Filters for Wireless Communication: Theory Design and Application, Springer, Berlin, 2001.
[2] M.T. Sebastian, Dielectric Materials for Wireless Communications, Elsevier Publishers, Oxford, U.K., 2008.
[3] K. Wakino, Miniaturization techniques of microwave components for mobile communications systems-using low loss dielectrics, Ferroelectr. Rev. 22 (2000) 1–49.
[4] M.T. Sebastian, S. Solomon, R. Ratheesh, J. George, P. Mohanan, Preparation, characterization, and microwave properties of $RETiNbO_6$ (RE=Ce, Pr, Nd, Sm, Eu, Gd, Tb, Dy, Y, and Yb) dielectric ceramics, J. Am. Ceram. Soc. 84 (2001) 1487–1489.
[5] K.P. Surendran, M.R. Varma, P. Mohanan, M.T. Sebastian, Microwave dielectric properties of $RE_{1-x}RE'_xTiNbO_6$ [RE=Pr, Nd, Sm; RE'=Gd, Dy, Y] ceramics, J. Am. Ceram. Soc. 86 (2003) 1695–1699.
[6] J.J. Bian, Y.Z. Li, L.L. Yuan, Structural stability and microwave dielectric properties (1-x)$Ln_{1/3}NbO_3$-x$Ln_{2/3}TiO_3$ (Ln: la, Nd; 0≤x≤0.8), Mater. Chem. Phys. 116 (2009) 102–106.
[7] J. Zhang, R.Z. Zuo, A novel self-composite property-tunable $LaTiNbO_6$ microwave dielectric ceramic, Mater. Res. Bull. 83 (2016) 568–572.
[8] A.C. Larson, R.B. Von Dreele, General Structural Analysis System (GSAS), LANSCE, MS-H805, Los Alamos, New Mexico, 1994.
[9] B.H. Toby, EXPGUI, a graphical user interface for GSAS, J. Appl. Crystallogr. 34 (2001) 210–213.
[10] B.W. Hakki, P.D. Coleman, A dielectric resonator method of measuring inductive capacities in the millimeter range, IEEE Trans. Microw. Theory Tech. 8 (1960) 402–410.
[11] W.E. Courtney, Analysis and evaluation of a method of measuring the complex permittivity and permeability of microwave insulators, IEEE Trans. Microw. Theory Tech. 18 (1970) 476–485.
[12] V.I. Strakhov, O.V. Mel'nikova, M. Dib, Phase diagram for the system $LaNbO_4$-TiO_2, Inorg. Mater. 27 (1991) 495–498.
[13] A. Golobič, S.D. Škapin, D. Suvorov, A. Meden, Solving structural problems of ceramic materials, Croat. Chem. Acta 77 (2004) 435–446.
[14] V.B. Alexandrov, Crystal texture of aeschynite, Dokl. Akad. Nauk SSSR 142 (1962) 181–184.
[15] R.D. Shannon, Revised effective ionic radii and systematic studies of interatomic distances in halides and chalcogenides, Acta Cryst. A 32 (1976) 751–767.
[16] S. Sumi, P.P. Rao, M. Deepa, P. Koshy, Electrical conductivity and impedance spectroscopy studies of cerium based aeschynite type semiconducting oxides: $CeTiMO_6$ (M= Nb or Ta), J. Appl. Phys. 108 (2010) 063718.
[17] S.K. Singh, S.R. Kiran, V.R.K. Murthy, Structural, Raman spectroscopic and microwave dielectric studies on spinel $Li_2Zn_{(1-x)}Ni_xTi3O8$ compounds, Mater. Chem. Phys. 141 (2013) 822–827.
[18] C.W.A. Paschoal, R.L. Moreira, C. Fantini, M.A. Pimenta, K.P. Surendran, M.T. Sebastian, Raman scattering study of $RETiTaO_6$ dielectric ceramics, J. Eur. Ceram. Soc. 23 (2003) 2661–2666.

[19] L. Xue, W.L. Gong, A study on Raman and photoluminescence spectra of the aeschynite group minerals, Spectrosc. Spectr. Anal. 20 (2000) 827–829.
[20] Y. Repelin, E. Husson, H. Brusset, Etude par spectroscopies d'absorption ir et de diffusion Raman des composés $A^{II}B_2^{V}O_6$ de structure de type "blocs 1×2"—I. Etude du niobate de baryum $BaNb_2O_6$, Spectrochim. Acta A 35 (1979) 937–948.
[21] M.Y. Chen, C.T. Chia, I.N. Lin, L.J. Lin, C.W. Ahn, S. Nahm, Microwave properties of $Ba(Mg_{1/3}Ta_{2/3})O_3$, $Ba(Mg_{1/3}Nb_{2/3})O_3$ and $Ba(Co_{1/3}Nb_{2/3})O_3$ ceramics revealed by Raman scattering, J. Eur. Ceram. Soc. 26 (2006) 1965–1968.
[22] Q.W. Liao, L.X. Li, Structural dependence of microwave dielectric properties of ixiolite structured $ZnTiNb_2O_8$ materials: crystal structure refinement and Raman spectra study, Dalton Trans. 41 (2012) 6963–6969.
[23] J. Zhang, R.Z. Zuo, Y. Cheng, Relationship of the structural phase transition and microwave dielectric properties in $MgZrNb_2O_8$-TiO_2 ceramics, Ceram. Int. 42 (2016) 7681–7689.
[24] D. Zhou, L.X. Pang, J. Guo, Z.M. Qi, T. Shao, Q.P. Wang, H.D. Xie, X. Yao, C.A. Randall, Influence of Ce substitution for Bi in $BiVO_4$ and the impact on the phase evolution and microwave dielectric properties, Inorg. Mater. 53 (2014) 1048–1055.
[25] M.T. Sebastian, R. Ubic, H. Jantunen, Low-loss dielectric ceramic materials and their properties, Int. Mater. Rev. 60 (2015) 392–412.
[26] M.T. Sebastian, H. Wang, H. Jantunen, Low temperature co-fired ceramics with ultra-low sintering temperature: a review, Curr. Opin. Solid State Mater. Sci. 20 (2016) 151–170.
[27] H.H. Xi, D. Zhou, H.D. Xie, B. He, Q.P. Wang, Raman spectra, infrared spectra, and microwave dielectric properties of low-temperature firing $[(Li_{0.5}Ln_{0.5})_{1-x}Ca_x]MoO_4$ (Ln=Sm and Nd) solid solution ceramics with scheelite structure, J. Am. Ceram. Soc. 98 (2015) 587–593.
[28] F. Gervais, P. Echegut, Incommensurate Phases in Dielectrics, North Holland, Amsterdam, 1986.
[29] K.P.F. Siqueira, R.L. Moreira, A. Dias, Synthesis and crystal structure of lanthanide orthoniobates studied by vibrational spectroscopy, Chem. Mater. 22 (2010) 2668–2674.
[30] R.L. Moreira, A. Feteira, A. Dias, Raman and infrared spectroscopic investigations on the crystal structure and phonon modes of $LaYbO_3$ ceramics, J. Phys. Condens. Matter 17 (2005) 2775–2781.
[31] N.G. Teixeira, R.L. Moreira, R.P.S.M. Lobo, M.R.B. Andreeta, A.C. Hernandes, A. Dias, Raman and infrared phonon features in a designed cubic polymorph of $CaTa_2O_6$, Cryst. Growth Des. 11 (2011) 5567–5573.
[32] D.D. Meneses, G. Gruener, M. Malki, P. Echegut, Causal voigt profile for modeling reflectivity spectra of glasses, J. Non-Cryst. Solids 351 (2005) 124–129.
[33] D. Zhou, W.B. Li, J. Guo, L.X. Pang, Z.M. Qi, T. Shao, H.D. Xie, Z.X. Yue, X. Yao, Structure, phase evolution, and microwave dielectric properties of $(Ag_{0.5}Bi_{0.5})(Mo_{0.5}W_{0.5})O_4$ ceramic with ultralow sintering temperature, Inorg. Chem. 53 (2014) 5712–5716.
[34] J. Guo, C.A. Randall, D. Zhou, G. Zhang, C. Zhang, B. Jin, H. Wang, Correlation between vibrational modes and dielectric properties in $(Ca_{1-3x}Bi_{2x}\Phi_x)MoO_4$ ceramics, J. Eur. Ceram. Soc. 35 (2015) 4459–4464.